Int J Adv Manuf Technol (2017) 93:1829–1842
DOI 10.1007/s00170-017-0613-6

ORIGINAL ARTICLE

The cutting force and defect analysis in milling of carbon fiber-reinforced polymer (CFRP) composite

Yanli He[1] · **Huanan Qing**[1] · **Shengguang Zhang**[1] · **Dazhen Wang**[1] · **Shengwei Zhu**[1]

Received: 3 October 2016 / Accepted: 5 June 2017 / Published online: 22 June 2017

Abstract Carbon fiber-reinforced polymer (CFRP) composite parts are usually made as near-net shape in aerospace and astronautic industry. However, mechanical machining such as milling is often required for part finishing in order to meet the dimensional accuracy before assembly. The milling process is vulnerable to damage like fiber breakage and pullout, and delamination. The cutting force is generally recognized as an indicator of machinability for milling of CFRP. In this study, slot milling of unidirectional CFRP was conducted with different cutting orientations and conditions. The patterns of cutting force and resulting defects along with the inherent mechanism are investigated. A mechanistic milling force model is proposed in which the specific cutting energies are modeled and calibrated considering the instantaneous chip thickness, fiber cutting angle, and cutting speed. The model is applicable to force prediction in milling both unidirectional CFRP and multi-directional CFRP.

Keywords Milling · CFRP · Cutting force · Specific cutting energy · Mechanistic modeling · Defect

1 Introduction

Mechanical machining, such as milling, is an important approach in the final processing of carbon fiber-reinforced polymer (CFRP) in order to meet the dimensional requirements [1]. However, machining CFRP is vulnerable to damage such as fiber breakage and pullout, resin degradation, and delamination due to its multi-phase and anisotropic nature [1–14]. The research on the milling of CFRP or glass fiber-reinforced polymer (GFRP) composite during the past years showed that the factors of FRP workpiece material, fiber orientation, cutting parameters, tool geometry, and tool material have an essential influence on the machining process. In the earlier work by Hocheng et al. [2], milling experiment shows that fiber orientation plays a significant role in the chip shapes, surface roughness, and cutting forces. In the experiments of milling CFRP and GFRP using cemented carbide end mills by Davim and Reis [3, 4], the influence of cutting parameters on the machining output is studied. Generally, both machining force and surface roughness increase with feed rate and decrease with cutting speed, while delamination factor increases with feed rate and also with cutting speed, both factors having a statistical and physical significance. Similarly, milling experiment on unidirectional GFRP (UD-GFRP) with end mill by Azmi et al. [5] shows the same results, with feed rate having the most dominant role in surface roughness and resultant machining force. The end milling of CFRP panel with 0°/45° layup by Khairusshima et al. [6] and milling of 0°/90° woven GFRP by Erkan et al. [7] also showed similar results about surface roughness and damage factor respectively, and the use of chilled air could result to less tool wear and delamination as well as a better surface quality. The experiment of milling with different cutters by Chatelain and Zaghbani [8] shows that adding features to the standard geometry significantly affects the milling forces, with the grooved geometry inducing a qusai-null thrust force accompanied by less fluctuation of the feed force and normal force. Sheikh-Ahmad et al. [9] studied the trimming of CFRP panel made of plain weave fibers using burr router bits in up milling and found that

✉ Yanli He
heyl@nwpu.edu.cn

[1] Key Laboratory of Contemporary Design and Integrated Manufacturing Technology, Ministry of Education, School of Mechanical Engineering, Northwestern Polytechnical University, Xi'an, 710072 Shaanxi, People's Republic of China

topography of the machined surface is dependent on cutting conditions as well as fiber orientation. Both longitudinal surface roughness and the average delamination depth increase with feed rate and decrease with spindle speed. Best machined surface quality can be achieved by the smallest feed and largest cutting speed, corresponding to the smallest effective chip thickness. Haddad et al. [10] found that the fiber pullout defect is closely related to fiber orientation when trimming multi-directional CFRP using a burr tool. Hosokawa et al. [11] conducted side milling on multi-directional CFRP plate using tools with different coatings and helix angles and found that the effect of geometry is more significant than that of coatings of end mills. Higher helix angle can induce smaller tangential and normal cutting forces, smoother surface with less pullout, and delamination, but more fluffing area. Hintze et al. [12–14] found that the occurrence of delamination of unidirectional CFRP and the fiber overhang length are related to the critical fiber cutting angle, and the delamination can be modeled considering the geometric and mechanical properties of CFRP, tool geometry, and fiber cutting angle. For milling CFRP with woven fabric, the fiber undulation angle and thickness of the top matrix layer have the main influence on delamination.

Similar to the FRP drilling process where thrust force is an important cause of damage and defects [15], cutting force is recognized as an important indicator of machinability for milling of FRP in most existing experiment. The cutting force reflects the load exerted on the FRP workpiece during milling, and the damage observed on the final part is a combination of force profile and amplitude characteristics. There is an essential requirement for reducing the cutting force so as to avoid damages. For this purpose, cutting force modeling and prediction for the machining of FRP have drawn much interest in the literature during past years. Many early orthogonal cutting experiments studied the machining mechanism such as chip formation and damage as well as the cutting force models [16–18]. In the earlier work by Bhatnagar et al. [18], shear plane was assumed along the fiber direction and the shear plane theory was used as an approximation to predict the forces in cutting FRP. The friction angle was calculated based on Merchant's circle using the force data. For validation of the model, the shear strength was calculated for different fiber orientations and compared with those obtained through Iosipescu shear test. Results show reasonable agreement with experiments for fiber orientation between 10° and 60°. Later, Zhang et al. [19] proposed a mechanics model for predicting forces in the orthogonal cutting of unidirectional FRPs with fiber orientation varying from 0° to 90°. Three cutting regions (i.e., chipping, pressing, and bouncing regions) were identified and models were proposed for each region according to their respective mechanisms. This model considered the influence of tool geometry including rake angle, clearance angle, and nose radius on the cutting process. A maximum error of 37% for vertical cutting force prediction and 27% for horizontal force were observed when compared to experiment. This is acceptable considering the mechanics model nature. Jahromi and Bahr [20] later proposed an energy-based analytical model to predict the cutting forces in orthogonal machining of unidirectional FRP (UD-FRP) with fiber orientations above 90°.

Mechanistic modeling approach which is widely used in metal cutting [21] was also applied for the analysis of orthogonal cutting of UD-FRP [1]. In this model, cutting force is expressed by specific cutting energy (or specific cutting force) and the chip load. From the machining experiment, the calculated specific energy for milling FRP is critically dependent on fiber orientation, particularly for the horizontal cutting force coefficient which always increases obviously with increasing fiber orientation. This is explained because the fiber cutting angle plays an important role in chip mechanism. Depth of cut also shows a strong influence on cutting force coefficient, with specific cutting force increasing exponentially with a decrease in the depth of cut [1]. Schulze et al. [22] studied the specific machining forces in machining composites reinforced by short glass fiber with random orientation (quasi-homogeneous) nature. Results show that specific cutting forces decrease with increasing cutting thickness while increase with increasing cutting edge radius. Multivariate regression model was then proposed for calculating specific cutting/passive forces and direction of resultant forces. Both analytical model and mechanistic model approaches were also applied in other types of FRP machining process. For example, Chang [23] proposed a mechanical cutting force model for turning of GFRP with assumption of energy and power consumption and Merchant's model. Based on experimental force data, the empirical constants of the mechanical force model was estimated and further used for cutting force prediction. Besides, Chandrasekharan et al. [24] and Langlela et al. [25] proposed mechanistic force models for force prediction in drilling FRP.

Due to the complexity of the milling process, most existing research works on milling forces were based on mechanistic model. This approach could reveal more force mechanism than the pure empirical models [26–28] which are obtained simply by regression of force data. Puw and Hocheng [29] proposed a mechanistic modeling for milling of unidirectional polymer composites. Specific cutting energy function was obtained from planning experiments. However, this model was limited to the condition that feed direction is parallel or perpendicular to the of fiber orientations. In helical milling of unidirectional CFRP by Wang and Qin [30], cutting force coefficients were identified with an average-based method rather than instantaneous force. The effects of fiber cutting angle and chip thickness on cutting force coefficients were not considered. Sheikh-Ahmad et al. [31] developed a cutting force prediction model for milling FRP with straight edge tools. The specific cutting energy was treated as continuous function of fiber orientation and chip thickness. Both multiple

regression analysis and committee neural network approximation were applied for the specific energy approximation. To address helix angle effect, Kalla et al. [32] developed mechanistic cutting force model for milling of CFRP with a helical end mills by dividing the cutting edge into a finite number of disks along axis. The tangential and radial cutting force coefficients for each disk are predicted by neural networks. The elemental cutting forces are calculated from cutting force coefficients and orthogonal to oblique transformation method. In the mechanistic cutting force model by Karpat et al. [33], the cutting force coefficient was represented as a sine function based on a least squares optimization algorithm. However, this function does not consider full influential factors such as chip thickness and cutting speed.

This study conducted slot milling experiment on unidirectional CFRP with different cutting orientations and conditions. The patterns of the cutting force, the defects, and the mechanisms are investigated. A mechanistic milling force model incorporating instantaneous chip thickness, cutting speed, and fiber orientation is proposed. The model is applicable to force prediction in milling both unidirectional CFRP (UD-CFRP) and multi-directional CFRP. The predicted milling force has a reasonable agreement with experiment. This work can be applied in the area of process planning and defect control in milling CFRP in industry.

2 Cutting experiment

The milling experiments were conducted on a four-axis vertical machining center (YHVT850Z) with CNC Siemens-840D control system. The experiment setup is shown in Fig. 1.The CFRP laminate was made of 43 layers of unidirectional long carbon fabric/epoxy resin prepregs (TC35-12K/150) subjected to an autoclave process. The laminate composite has a thickness of 6 mm and approximate 60% fibers in volume. For validation purposes, the milling was also conducted on a multi-directional laminate made with 90°/0° layup to verify the flexibility of the model. The customized two-straight-flute carbide end mill was designed and ground to conduct the experiments. The tool has the diameter of 8 mm, a rake angle of 6°, and a clearance angle of 10°, with zero helix angle.

The CFRP laminate was cut into 230 mm × 90 mm rectangular pieces with the fibers parallel to lengthwise direction. The workpiece penal was fixed at both ends by a clamp. The milling forces were measured by a three-axis piezoelectric dynamometer (Kistler9265B) attached between the workpiece and the machine table. The signal was collected and amplified by Kistler 5019A multi-channel amplifiers before transferred to National Instruments (NI) data acquisition (DAQ) card. The signal was continuously sampled with a frequency of 20,000 Hz. No coolant was used during the milling, and a vacuum (KARCHER) was used to collect the hazardous dust to avoid its health and environmental effects.

After machining, the quality of machined surfaces were analyzed using a surface roughness tester (Mahr MarSurf XT20) and a scanning electron microscope (SEM, model HITACHI SU3500). The average surface roughness "Ra" was used. A 5.6 mm traverse length and a 0.8 mm cut-off length were used in roughness measurement. An optical surface metrology instrument (Alicona Infinite Focus Microscope G4) was also used to examine the surface profile and topography.

As shown in Fig. 2, the angle measured counterclockwise from tool feed direction to fiber direction is referred as fiber orientation angle (φ). Four typical fiber orientation angles (e.g., 0°, 45°, 90°, 135°) are demonstrated in the figure. The rotation angle (θ) is used to describe the position of the cutting edge. An edge starts milling at $\theta = 0°$ and exits milling at $\theta = 180°$ in slot milling. In the figure, the cutting between $0° < \theta < 90°$ corresponds to up milling while turns into down milling for $90° < \theta < 180°$. The fiber cutting angle (β), measured counterclockwise from cutting velocity of the engaged edge to fiber direction, changes continuously as the rotary motion of cutting tool during the milling.

Figure 2 also shows the variation of fiber cutting angle (β) with respect to φ and θ. The relation is expressed as Eq. (1) [12, 33]. Basically, β increases from the value of φ from initial cutting. Whenever it reaches 180°, it periodically increases starting from zero again and finally reaches φ at exit of cutting

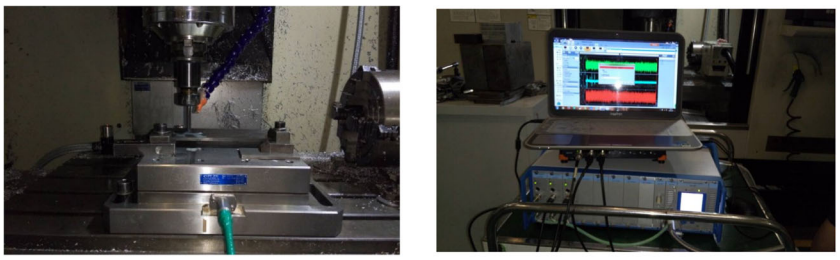

(a) (b)

Fig. 1 The experiment configuration. **a** Setup. **b** Amplifier

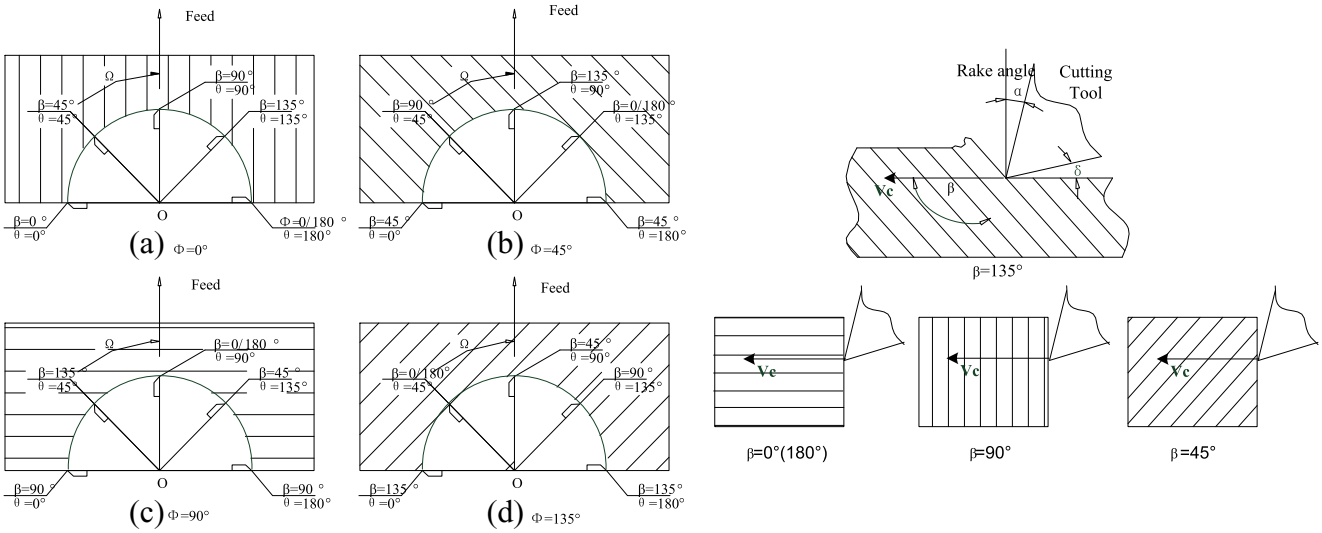

Fig. 2 The angle definition

$$\beta = \varphi + \theta \ \ if \ \ \beta \geq 180 \ \ then \ \ \beta = \mathrm{mod}(\beta, 180) \tag{1}$$

The cutting parameters are listed in Table 1. Different cutting and feed speeds were tested for each fiber orientation in order to obtain the influence of cutting parameters on specific cutting energy for the tool-workpiece combination. To isolate the individual influence of cutting speed, the feed per tooth was set constant (0.02 mm/z) while the feed rate per minute varies with spindle speed levels (Ω). The influence of cutting speed can be observed intuitively when comparing the forces of the same fiber orientation, at the same rotation angle where they have exactly the same fiber cutting angle and uncut chip thickness. In addition, the axis depth of cut was kept at 2 mm in the experiments.

In a cutting test, different fiber orientation angles are achieved by adjusting the feed direction with respect to the fixed fiber direction of the workpiece, as shown in Fig. 3.

3 Cutting force analysis

In the stable cutting force records in different fiber orientations, due to zero helix angle of the cutting tools, the axis cutting forces are close to zero and appear as a horizontal line when compared to other force components and thus were omitted.

All the measured cutting forces are represented in the dynamometer coordination system (X_d, Y_d, Z_d). To have a proper comparison and facilitate data processing, the cutting forces measured in dynamometer coordination were transformed to corresponding feed coordination (X, Y, Z) for different tests, where X and Y aliens feed and normal direction, respectively, as shown in Fig. 3. In this configuration, forces recorded by dynamometer are transformed through vector transformation law shown in Eq. (2),

$$\begin{Bmatrix} F_x \\ F_y \\ F_z \end{Bmatrix} = \begin{bmatrix} l_1 & m_1 & n_1 \\ l_2 & m_2 & n_2 \\ l_3 & m_3 & n_3 \end{bmatrix} \begin{Bmatrix} F_x \\ F_y \\ F_z \end{Bmatrix}^d \tag{2}$$

with sub index "d" denoting the original force records by dynamometer and (l_1,m_1,n_1) denoting the direction cosines of unit X with respect to (X_d, Y_d, Z_d) axes. Similarly, (l_2, m_2, n_2) and (l_3, m_3, n_3) denote the direction cosines of Y and Z with respect to (X_d, Y_d, Z_d) axes.

For each test, five samples at different time windows were identified and averaged to eliminate dynamic oscillation of signal due to, e.g., the eccentric tool setup. The feed and normal forces results are shown in Fig. 4. It is noted that there are two possible tool movement directions to choose from in order to achieve the same fiber orientation angle (e.g., tool move left rather than right for 0° orientation in Fig. 3). However,

Table 1 Cutting parameters

Spindle speed Ω (rpm)	Depth of cut a_p (mm)	Feed f (mm/min)	Fiber orientation angle φ(deg)
3000/4000/5000	2	120/160/200	0/45/90/135

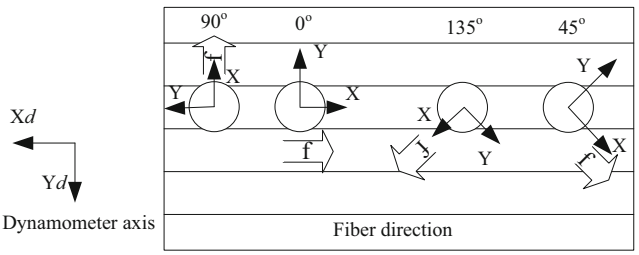

Fig. 3 Cutting plan achieving different fiber orientation angles

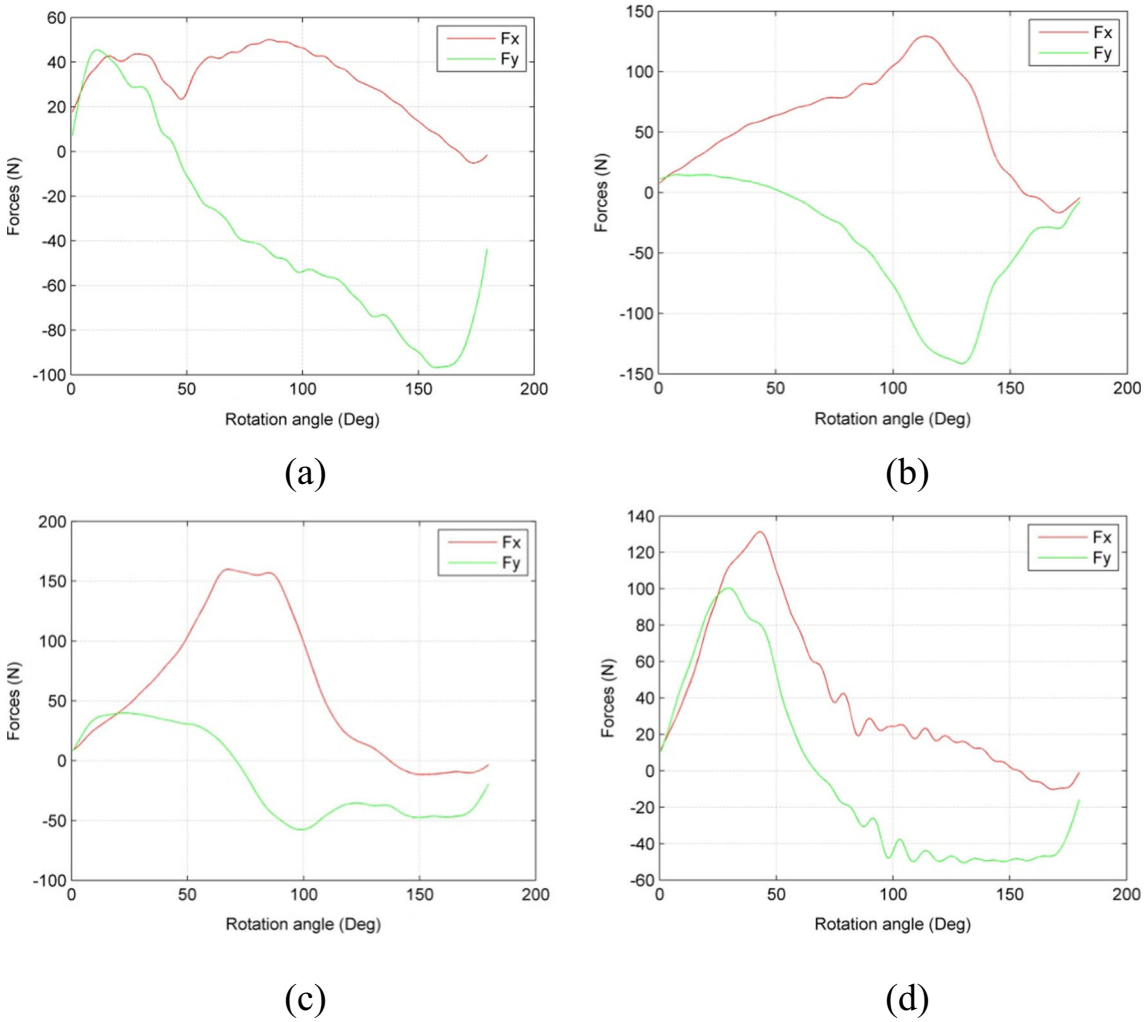

Fig. 4 Feed and normal forces in different fiber orientations (3000 rpm). **a** 0°. **b** 45°. **c** 90°. **d** 135°

theoretically, Eq.(2) will ensure exactly the same transformed feed and normal forces since both the matrix and the original force data records will be changed.

Unlike in metal cutting, the cutting forces of one tooth pass show different patterns in different fiber orientations. In all orientations, *Fx* increases and then drops, reaching a small negative value at the later stage. Peak *Fx* in 90° fiber orientation has the largest magnitude, and the smallest peak magnitude is observed in 0° orientation. The peak *Fx* in 45° and 135° orientations are close to each other, while tool rotation angles corresponding to peak force are different. *Fy* also increase from zero and drops to negative value before reaching zero again. The peak *Fy* value as well as the rotation angle reaching the peak is different among the four orientations. This shows that fiber orientation angle (and in consequence, the combined effects of fiber cutting angle and chip thickness) plays an important role in cutting force pattern.

To reveal the mechanism of cutting forces, *Fx* and *Fy* in feed coordination are further related to tool acting forces in tangential and radial components, i.e., *Ft* and *Fr* in Fig. 5. The relationship is shown in Eq. (3), where the tool rotation angle θ is between 0° and 180°.

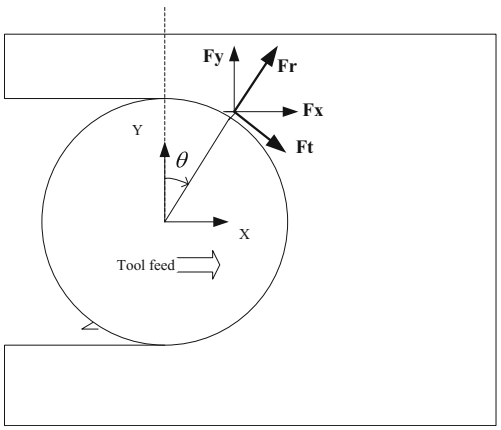

Fig. 5 Force in feed coordination and the tangential and radial components

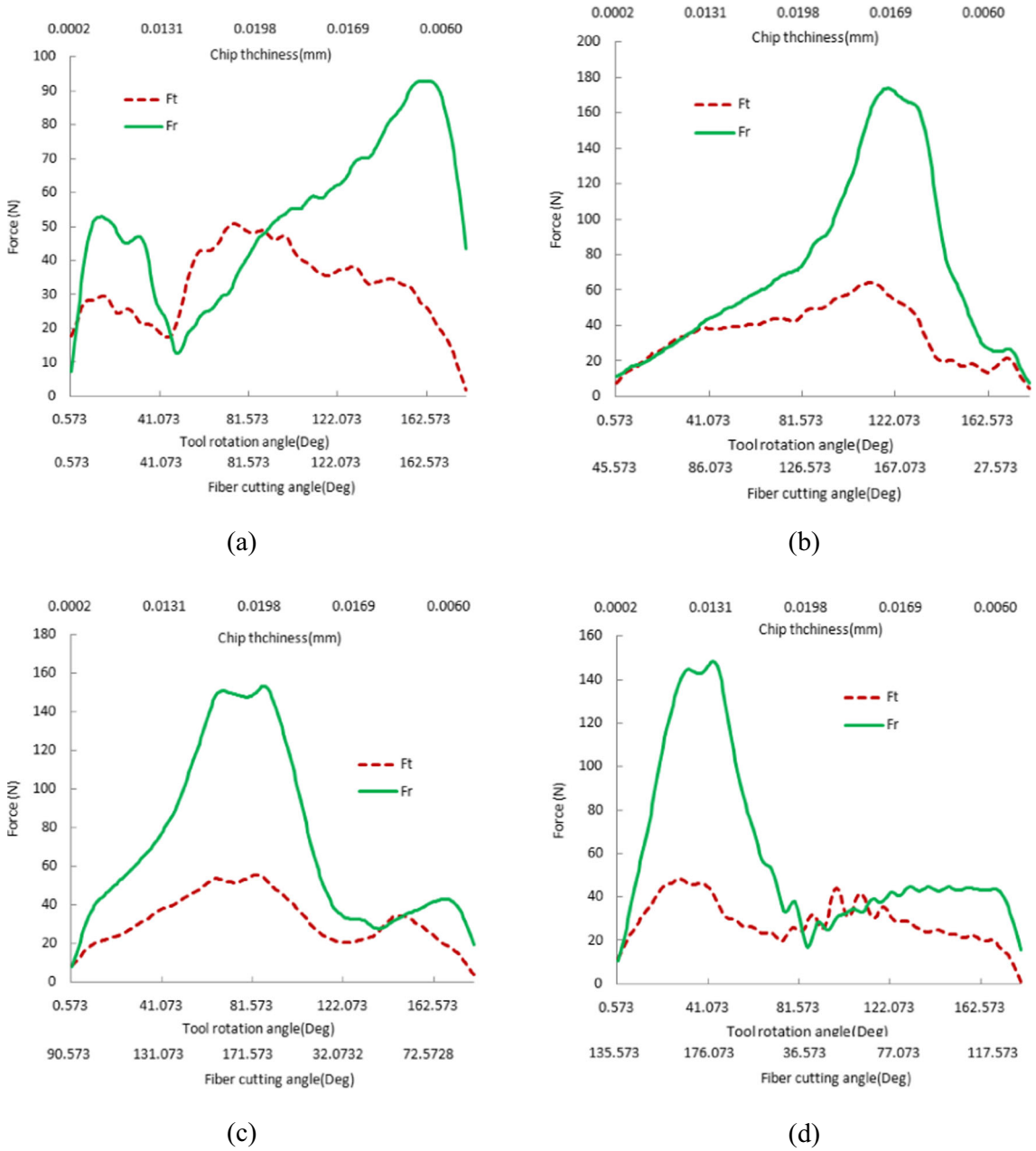

Fig. 6 The tangential and radial force components in one pass for different fiber orientations (3000 rpm). **a** 0°. **b** 45°. **c** 90°. **d** 135°

$$\begin{Bmatrix} F_t \\ F_r \end{Bmatrix} = \begin{bmatrix} \cos\theta & -\sin\theta \\ \sin\theta & \cos\theta \end{bmatrix} \begin{Bmatrix} F_x \\ F_y \end{Bmatrix} \tag{3}$$

The tangential and radial forces are shown in Fig. 6. Generally, the peak forces do not correspond to the maximum chip thickness point. And for a given cutting condition, the peak radial force is usually higher than the peak tangential force. These are in accordance with the observations in literature. Among the four orientations, the tool rotation angle corresponding to peak *Fr* decreases with increasing fiber orientation, but the fiber cutting angle remains similar (around 160°–170°). The fiber cutting angles corresponding to the trough *Fr* also remain similar (between 40°–50°).

In order to examine the effects of fiber cutting angle on the cutting force magnitude, the instantaneous cutting forces at three typical tool rotation angles (45°, 90°, and 135°) were recorded for each fiber orientation. Four typical fiber cutting angles are identified, and the instantaneous forces only at the same tool rotation angle were compared where they are assumed to have the same instantaneous chip thickness. The effect of fiber cutting angle is thus recognized, as shown in Fig. 7. The same comparison repeats three times in one tooth engagement cycle and they were also averaged so as to eliminate the errors in workpiece setup and

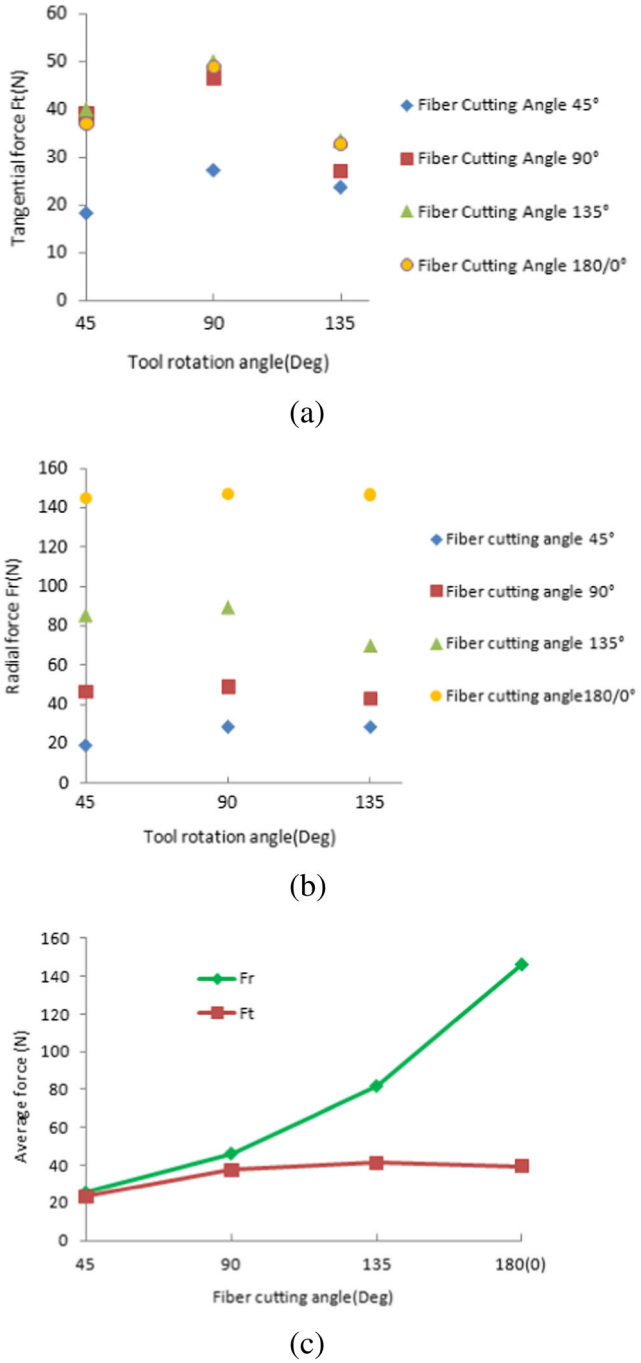

Fig. 7 Influence of fiber cutting angle on forces (3000 rpm). **a** *Ft*. **b** *Fr*. **c** Averaged force

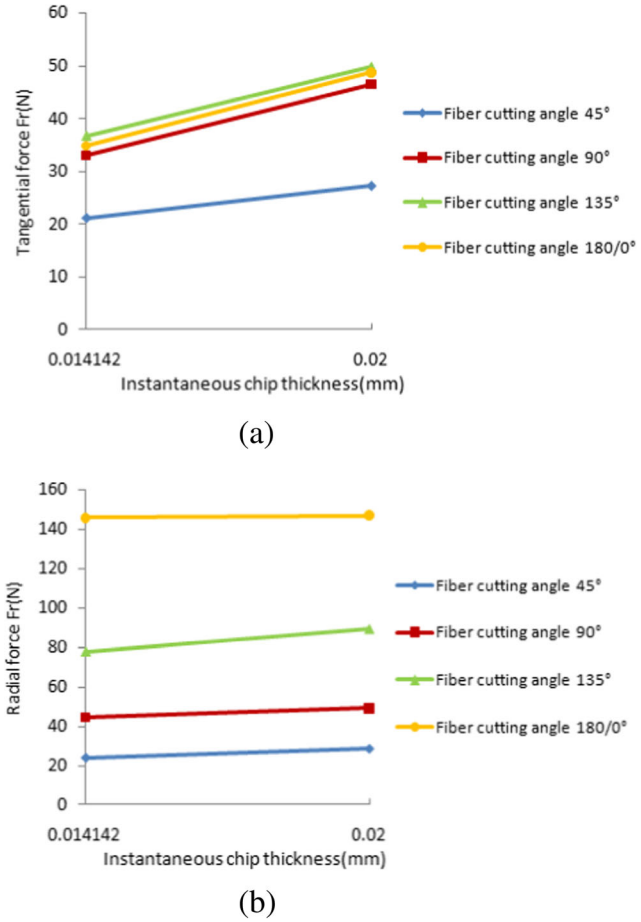

Fig. 8 Influence of chip thickness on cutting forces (3000 rpm). **a** *Ft*. **b** *Fr*

the measuring system. Result shows that among the four special fiber cutting angles (45°, 90°, 135°, 0/180°), the largest radial force appears on 0/180° angle, and the smallest one appears on 45°. The largest tangential force is observed on 135° fiber cutting angle, and the smallest one appears also on 45°. The 0/180° and 90° fiber cutting angles have the tangential forces magnitude close to each other.

In the four fiber orientation layouts (with the same cutting speed and feed, etc.), a particular fiber cutting angle always appeared three or four times, at different rotation angles corresponding to different chip thicknesses. The effect of chip thickness on cutting forces was studied, as shown in Fig. 8. Since the chip thickness at tool rotation angle 45° is assumed to be identical to that at rotation angle 135°, thus, an average force at the two angles was used. Both tangential force and radial force increase with increasing chip thickness. However, it seems that the influence is more obvious on tangential force than on radial force.

Cutting speed only has slight influence on *Ft* and *Fr*, with an example shown in Fig. 9. When spindle speed increases from 3000 to 5000 rpm, making the feed increase from 120 to 200 mm/min, the peak feed force and normal forces increase only slightly, and the resulting peak *Ft* and *Fr* also has a slight increasing tendency. This is perhaps because higher material deformation rate makes cutting more difficult as such higher cutting forces are obtained.

4 The damage patterns and the mechanism

Though the axial cutting force is very small in a slot milling test, the fluffing of the uncut and peeled up carbon fibers is

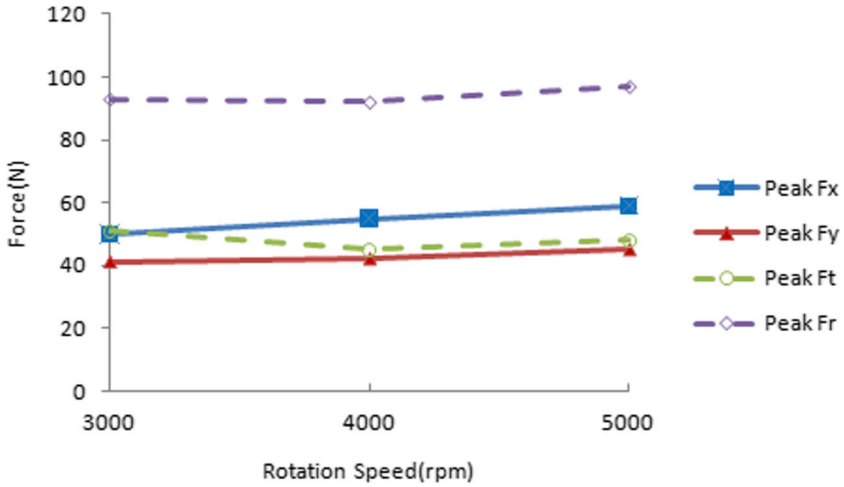

Fig. 9 The influence of cutting speed on cutting forces (fiber orientation 0°)

often observed in particular regions on the laminate top layer. As demonstrated in Fig. 10, the fluffing occurs at the right hand with respect to feed direction (down milling side) in 0° fiber orientation and at the left hand (up milling area) in 90° fiber orientation. For 135° fiber orientation, fluffing exists at both sides, and for 45° orientation, fluffing exists just in front of the tool feed direction.

Careful look shows the fluffing has a strong relationship with the fiber cutting angle. Severe fluffing exists when fiber cutting angle reaches 90° and beyond till 180°. When fiber cutting angle lies between 0° and 90°, there seems no or little fluffing left. These observations are also consistent with the experiment by Hocheng et al. [2] and Hintze et al. [12].

The pattern of fluffing depending on fiber cutting angle is explained by the chip formation mechanism in different fiber cutting angles. Figure 11 demonstrates the top layer of UD-CFRP laminate with respect to different cutting velocity. When fiber cutting angle is 0° or between 0° and 90°, the pushing effect of the tool tip is decomposed into the force along fiber direction. The fiber is subjected to axial compression force which results in crushing of the brittle fiber, so fibers are more easily removed with little chance of fluffing. This is proved by the experiment observation. For example, the fluffing free area of fiber orientation 45° (exit milling points) was examined in Fig. 12. The microcopy and SEM images show that the top layer and side wall surfaces are characterized by fiber crushing. However, the fiber is also under bending force component perpendicular to fiber towards the external of the machined surface at down milling point. This usually results in severe fiber bending and fiber/

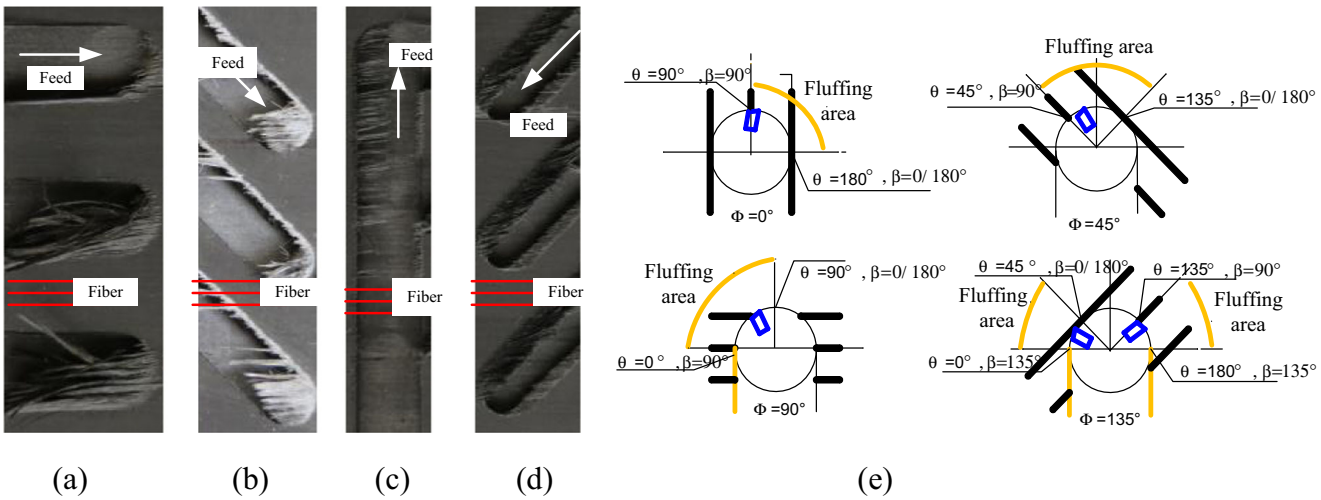

Fig. 10 The milling damage in different fiber orientation angles. **a** 0°. **b** 45°. **c** 90°. **d** 135°. **e** Damage sketch

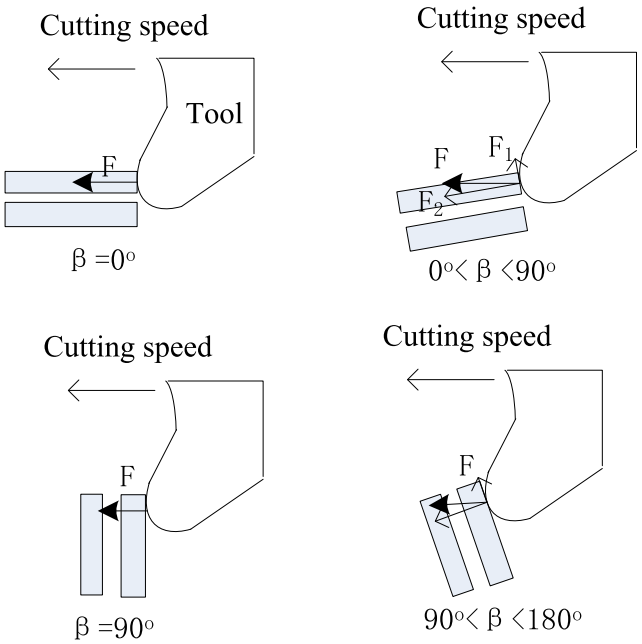

Fig. 11 The fluffing mechanism

matrix interface debonding because fibers get weaker support by the surrounding material in that direction. A relatively rough machined surface is thus generated. This is also observed in SEM image and additionally supported by the roughness test results in Fig. 13, which shows that the side wall surface at 45° fiber cutting angle (exit milling point) has the largest roughness value.

Further study shows that the fluffing intensities at up milling side and down milling side are not equal. A similar pattern can be observed in the literature [2]. One possible reason is that between 0° and 90°, with the increase of fiber cutting angle, the ratio between the compressing force components against the bending force components decreases, so 45°–90° region (region B) could have more chances of fluffing than 0°–45° region (region A). This explains why for the fiber orientation of 45° in Fig. 10, there exist, though very little, fluffing along the up milling side (the fiber cutting angle is entering region B at initial tool engagement), while down milling side is completely free of fluffing (leaving region A at the point of exit cutting).

When fiber cutting angle reaches 90°, the fibers are subject to instantaneous bending load. Above 90°, the instant effect can be decomposed into pulling and bending force. The tensile effects increase the machining difficulty. At these angles, it is difficult for the fiber be completely cut considering the tool rotation direction. The situation is even worse when the tool has a large radius or tool wear, in which the tool is more like "slipping" over the fiber rather than making a "cutting" effect. The uncut fibers are left forming serious fluffing on top layer as a consequence. This is supported by the observations in Fig. 14. In fluffing intensive area, there always exists pulling effect at the generated side surface and the delamination on top layer. However, the bending force perpendicular to fibers is towards internal of the workpiece at the exit milling point, and the fiber can be better supported in that direction. Thus, fiber bending and interface debonding are small and smoother machined surface can be achieved. This is also supported by the SEM image in Fig. 14 and the roughness test result in Fig. 13.

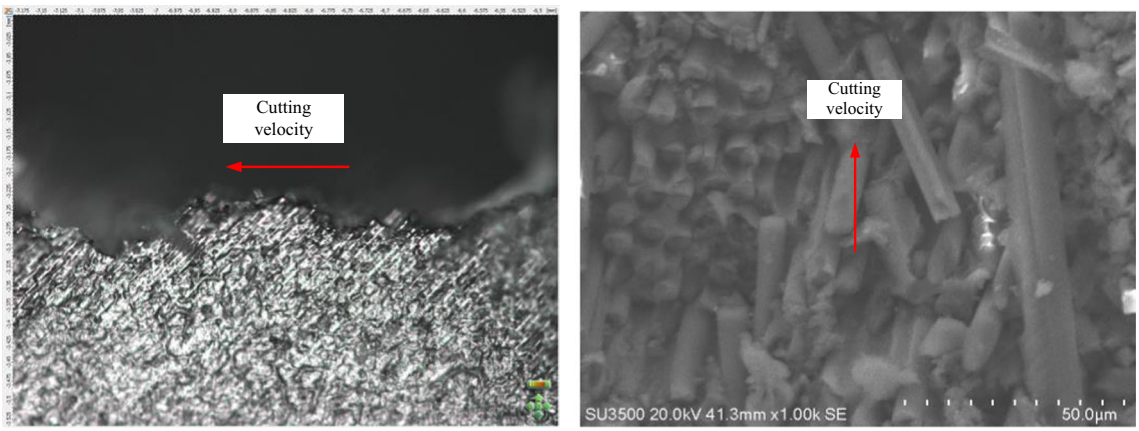

Fig. 12 Fluffing free area characterized by fiber crushing and debond (exit milling point of fiber orientation 45°, fiber cutting angle 45°, 3000 rpm). **a** Microscope image of top layer. **b** SEM image of generated side surface

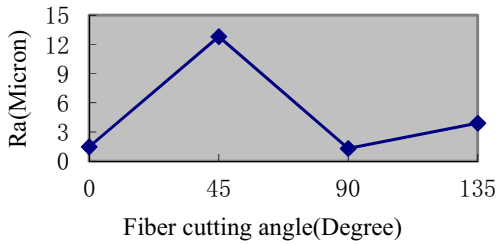

Fig. 13 Roughness of the side surface at different fiber cutting angles (measured at exit milling point of corresponding fiber orientation angle, 3000 rpm)

Again, among a fluffing-inducing region, it seems that 90°–135° region (region C) has more chances of inducing fluffing than 135°–180° (region D). For example, for fiber orientation 135° in Fig. 10, the fluffing in up milling side is less intensive than that induced in down milling side, because fiber cutting angle is getting larger than 135° (entering region D) at the point of tool engagement while is about reaching 135° at exit cutting point (exiting region C).

The intensity of fluffing/delamination damage increases with increasing speed, when the feed per tooth remains fixed. The damages of fiber orientation 90° with respect to cutting speed were demonstrated in Fig. 15. This is perhaps due to the increase in cutting forces with increasing cutting speed.

5 Milling force modeling

In slot milling process, the chip thickness at a certain location of the cutting edge is immersion and rotation dependent. As shown in Fig. 5, the instantaneous undeformed chip thickness is calculated by Eq. (4), where t_c is the chip thickness, f_t is the feed per tooth, and θ is the tool rotation angle.

$$t_c = f_t \sin\theta \tag{4}$$

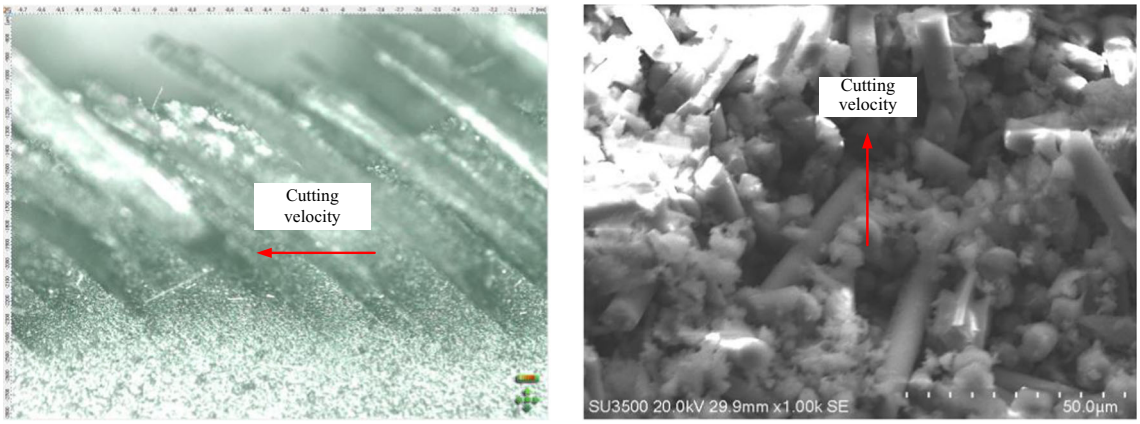

Fig. 14 The fluffing area characterized by inter-ply delamination (exit milling point of fiber orientation 135°, fiber cutting angle 135°, 3000 rpm). **a** Microscope image of top ply. **b** SEM image of generated side surface

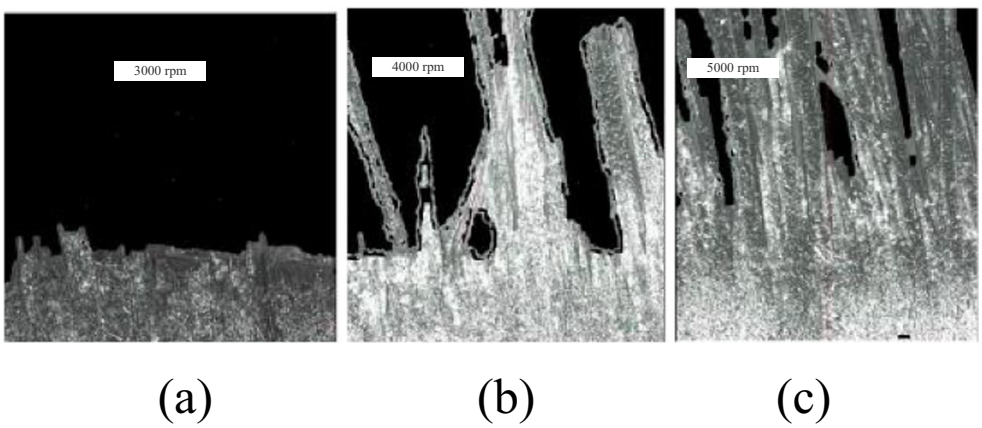

Fig. 15 The effects of cutting speed on fluffing/delamination (fiber orientation 90°, down milling). **a** 3000 rpm. **b** 4000 rpm. **c** 5000 rpm

In a mechanistic model, the radial and tangential cutting forces were defined as function of chip load (e.g., instantaneous chip thickness and depth of cut) and specific cutting force, as shown in Eq. (5), in which the *Kt* and *Kr* are tangential and radial cutting force coefficients and a_p is the depth of cut.

$$\begin{cases} F_t = a_p f_t \sin\theta \cdot K_t \\ F_r = a_p f_t \sin\theta \cdot K_r \end{cases} \quad (5)$$

The instantaneous *Kt* and *Kr* can be calculated from *Ft* and *Fr* using Eq. (5). The variation with the combined effects of chip thickness and fiber cutting angle are shown in Fig. 16.

Again, the *Kt* and *Kr* at three special rotation angles are identified in Fig. 17, and the influence of fiber cutting angle on the cutting force coefficient is also observed. Same to the phenomena in cutting forces, among the four special fiber cutting angles, 135° fiber cutting angle has the largest tangential force coefficients, and 45° fiber cutting angles have the smallest ones. Fiber cutting angle 0/180° has the largest radial force coefficient, followed by 135°, then 90°, and 45° has the smallest radial force coefficient.

The effects of chip thickness on *Kt* and *Kr* are shown in Fig. 18. As consistent with the observations in literature, there is a decreasing tendency with increasing chip

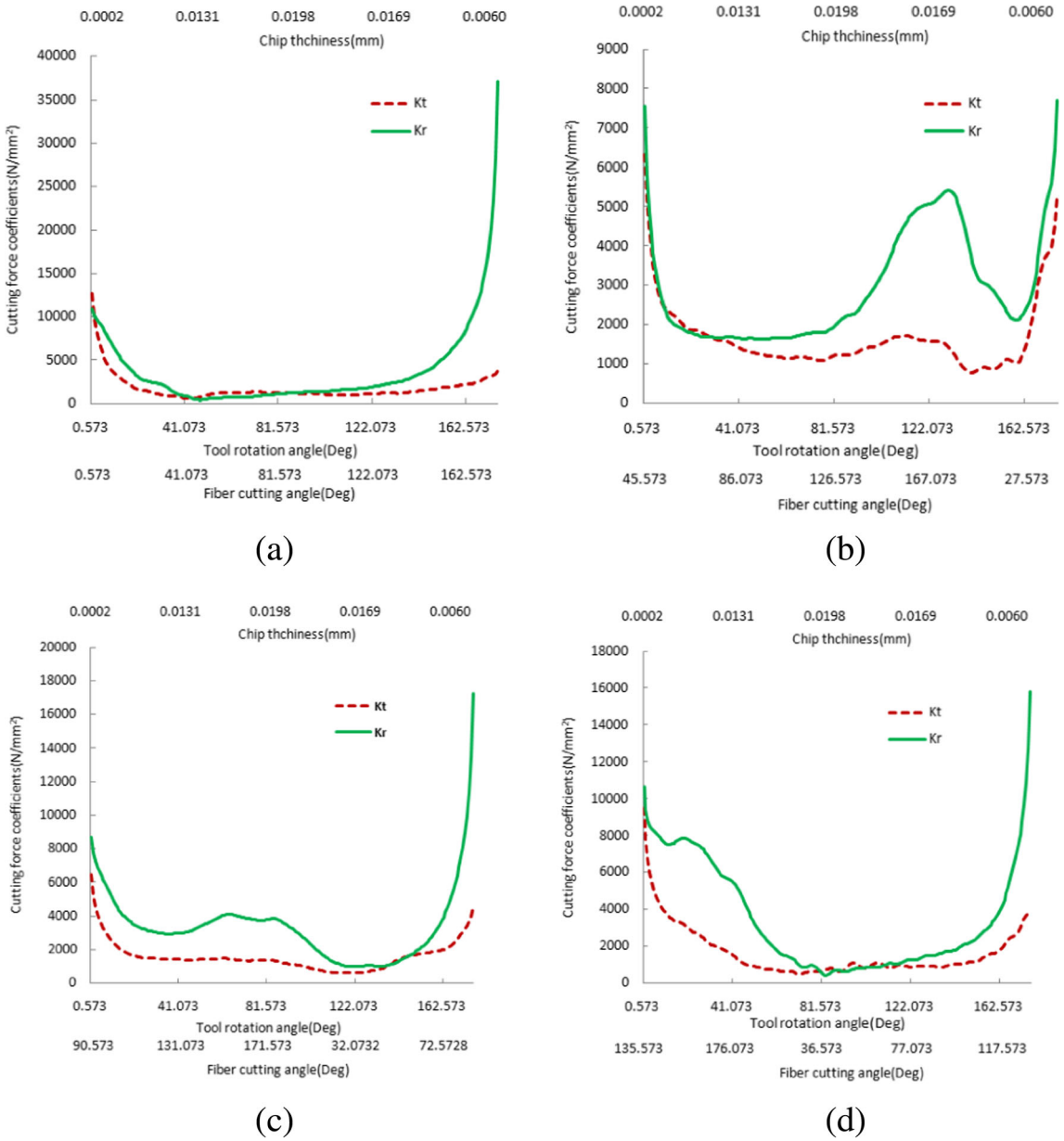

Fig. 16 *Kt* and *Kr* during milling different orientation laminate (3000 rpm). **a** 0°. **b** 45°. **c** 90°. **d** 135°

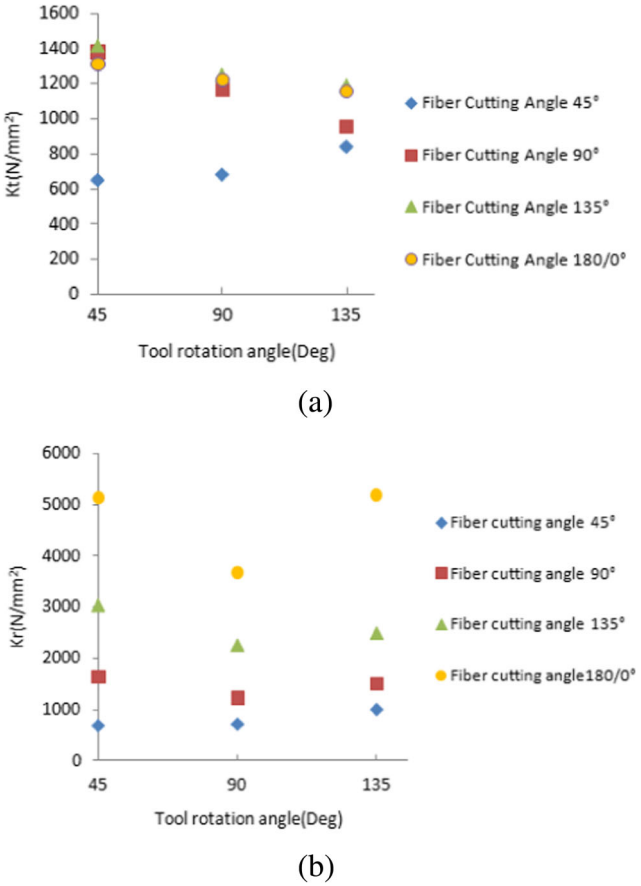

Fig. 17 Cutting force coefficients at different tool rotation angles (3000 rpm). **a** *Kt*. **b** *Kr*

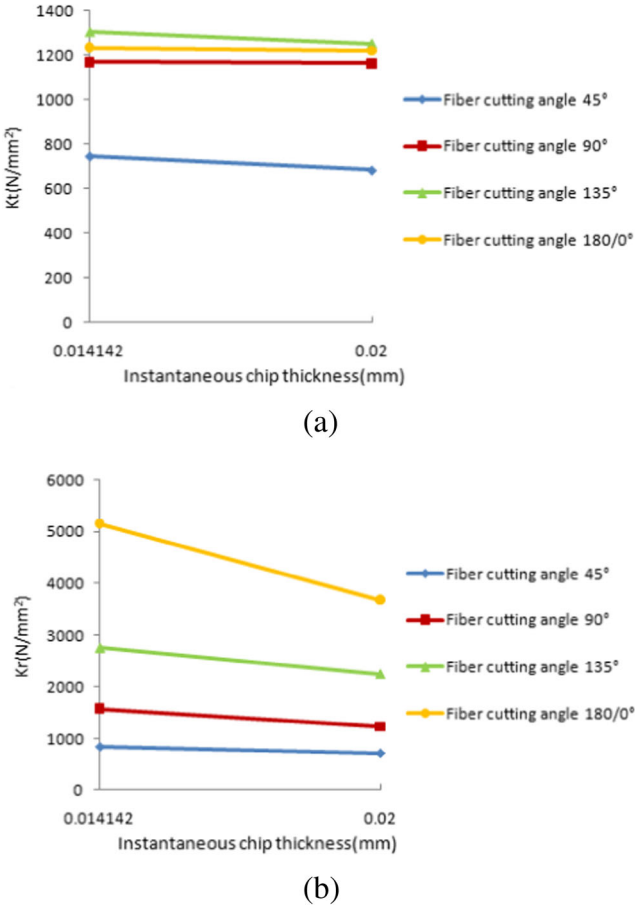

Fig. 18 Effects of chip thickness on cutting force coefficients (3000 rpm). **a** *Kt*. **b** *Kr*

thickness. As a result, the cutting force coefficients at 90° tool rotation angle are generally smaller than those at 45° or 135°.

The cutting speed only has marginal effects of on *Kt* and *Kr*, as implied in Fig. 9. With the increase of cutting speed ranging from 3000 to 5000 rpm, *Kt* and *Kr* have a slight increasing tendency.

In this study, *Kt* and *Kr* are modeled as the function of chip thickness t_c, cutting speed v, and fiber cutting angle β. A number of forms were analyzed and an example was shown in Eq. (6). It consisted of three product terms to account for the three independent influencing factors. Fiber cutting angle β is associated with sine function because 0° is identical to 180° from the cutting mechanism point of view, while using angle itself without sine function could introduce fluctuation in force prediction at 180° fiber cutting angle (due to the transition from 180° to 0°).

$$K = a_1 + a_2 \cdot t_c + a_3 \cdot \sin(2\beta + a_4) + a_5 \cdot v + a_6 \cdot t_c \cdot \sin(2\beta + a_7) + a_8 \cdot t_c \cdot v + a_9 \cdot v \cdot \sin(2\beta + a_{10}) + a_{11} \cdot {t_c}^2 + a_{12} \cdot \sin(3\beta + a_{13})^2 + a_{14} \cdot v^2 \quad (6)$$

Nonlinear regression is used to fit the parametric mathematical function to experimental *Kt* and *Kr* data. Through regression in Matlab, the coefficients in functions are established in Table 2. Using these coefficients, *Kt* and *Kr* under a given milling parameters can be predicted for the same tool-CFRP pair; then *Ft*, *Fr*, and *Fx*, *Fy* are further calculated.

The model was verified by subsequent milling experiment on unidirectional and multi-directional CFRP material with a 90°/0° layup using the same prepreg material. Milling of unidirectional CFRP was conducted with 4500 rpm and 180 mm/min feed at 30° fiber orientation, and milling of multi-directional laminate is conducted with 3500 rpm, 140 mm/min feed along the fiber of top ply, both with 2 mm of depth of cut. As suggested by Sheikh-Ahmad et al. [31], the forces in milling multi-directional CFRP laminate are predicted by superposition of the cutting forces required to independently machine each unidirectional ply in the laminate, as shown in Eq. (7), where a_p is the ply thickness and n is the number of plies being cut. The force is simulated as the combination of the instantaneous cutting force for simultaneously machining CFRP of 90° and 0° fiber orientations, each with half depth of cut. The results are shown in Fig. 19.

Table 2 Coefficients in functions

	a_1	a_2	a_3	a_4	a_5	a_6	a_7
Kt	5996.75	−486,610	694.403	322.288	−1354.51	−23,972.8	−15,668.4
Kr	11,465.5	−942,656	−3218.01	2355.52	−1813.52	102,151	−82,467.6
	a_8	a_9	a_{10}	a_{11}	a_{12}	a_{13}	a_{14}
Kt	47,757.3	−247.75	126.624	1.30639e+007	94.113	39.131	98.2255
Kr	41,176.7	401.439	447.238	2.63184e+007	−767.355	367.939	450.276

There is a reasonable agreement between the predicted cutting forces and experimental results.

$$F_t = \sum_{i=1}^{n} \left[K_t \cdot t_c \cdot a_p\right]_i$$
$$F_r = \sum_{i=1}^{n} \left[K_r \cdot t_c \cdot a_p\right]_i \quad (7)$$

6 Conclusion

Slot milling experiment was conducted on CFRP laminate using a two-straight-flute carbide milling tool. The patterns and the mechanism of cutting force as well as the induced damage were analyzed. A mechanistic force model was proposed for predicting instantaneous machining force when milling CFRP. The findings of this study can be summarized as below:

1. In one cutting cycle, the tangential and radial forces vary with the combined effects of instantaneous fiber cutting angle and chip thickness. Among the four special fiber cutting angles (45°, 90°, 135°, 0/180°), 0/180° fiber cutting angle has the largest radial force and specific cutting energy, and 135° has the largest tangential forces and specific cutting energy. Fiber cutting angle 45° corresponds to the smallest tangential forces and the smallest radial forces as well as the specific energies.
2. The fluffing and delamination concur during the milling process, and the mechanism is closely related to fiber cutting angle. Due to the force acting on the fiber in chip formation, 90° is the critical fiber cutting angle above which severe fluffing/delamination on top layer is induced because of fiber bending, and below which little or no fluffing is induced because of fiber crushing. However, the machined surface usually has a poor surface finish at fluffing free area. The damage also has an increasing tendency with increasing speed when the feed per tooth remains fixed.
3. Generally, the specific cutting forces decrease with instantaneous chip thickness but increase slightly with spindle speed at certain ranges. The specific cutting forces are modeled as the function of three influencing factors. The regression model shows reasonable agreement with experiment for milling UD-CFRP or multi-directional CFRP laminate.

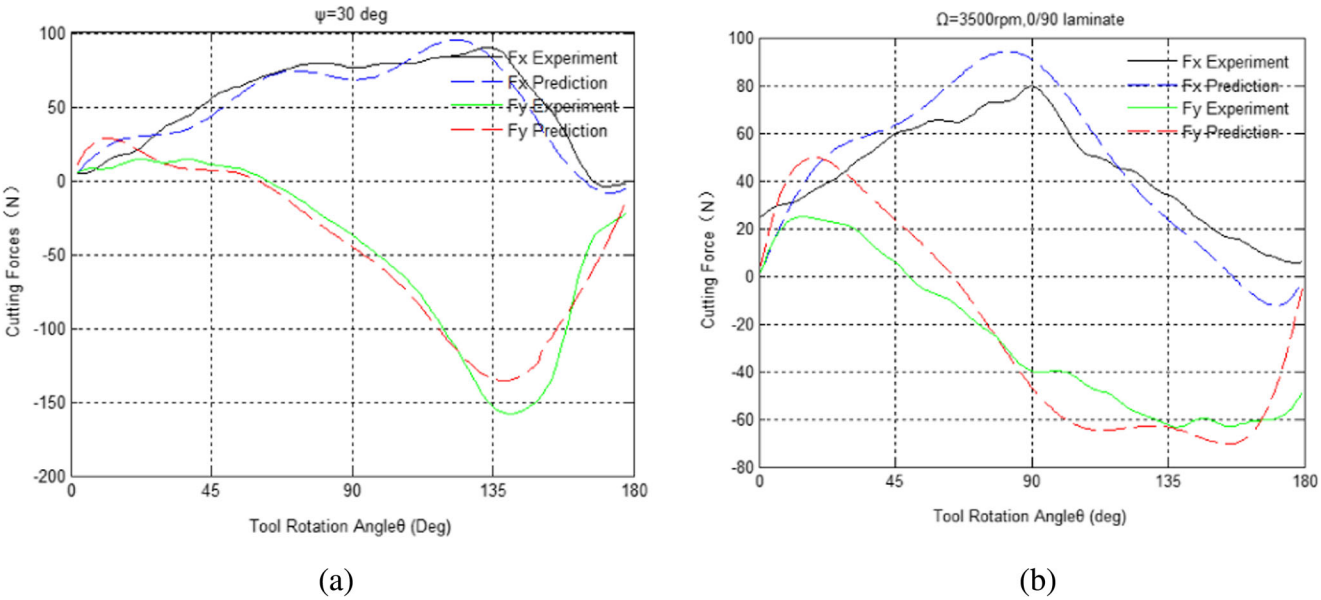

(a) (b)

Fig. 19 Experimental and predicted cutting forces. **a** Unidirectional CFRP, 4500 rpm, 30° orientation. **b** 90°/0° layup, 3500 rpm

Acknowledgments This work is partially supported by Science Foundation of NPU (Grant No. 3102015JCS05009) and Chinese Foreign Talents Introduction and Academic Exchange Program (Grant No. B13044).

References

1. Sheikh-Ahmad J (2009) Machining of polymer composites. Springer
2. Hocheng H, Puw HY, Huang Y (1993) Preliminary study on milling of unidirectional carbon fibre-reinforced plastics. Compos Manuf 4(2):103–108
3. Davim JP, Reis P (2005) Damage and dimensional precision on milling carbon fiber-reinforced plastics using design experiments. J Mater Process Technol 160(2):160–167
4. Davim JP, Reis P (2004) A study on milling of glass fiber reinforced plastics manufactured by hand-lay up using statistical analysis (ANOVA). Compos Struct 64(3–4):493–500
5. Azmi AI, Lin R, Bhattacharyya D (2013) Machinability study of glass fibre-reinforced polymer composites during end milling. Int J Adv Manuf Technol 64(1–4):247–261
6. Khairusshima MKN, Hassan CHC,Jaharah AG, Amin AKM, Idriss ANM (2013) Effect of chilled air on tool wear and workpiece quality during milling of carbon fibre-reinforced plastic. Wear 302(s 1–2):1113–1123
7. Erkan Ö, Işık B, Çiçek A, Kara F (2013) Prediction of damage factor in end milling of glass fibre reinforced plastic composites using artificial neural network. Appl Compos Mater 20(4):517–536
8. Chatelain JF, Zaghbani I (2012) A comparison of special helical cutter geometries based on cutting forces for the trimming of CFRP laminates. Int J Mech 6(1):52–59
9. Sheikh-Ahmad J, Urban N, Cheraghi H (2012) Machining damage in edge trimming of CFRP. Mater Manuf Processes 27(7), 802–808
10. Haddad M, Zitoune R, Bougherara H, Eyma F, Castanié B (2014) Study of trimming damages of CFRP structures in function of the machining processes and their impact on the mechanical behavior. Compos B: Eng 57(2):136–143
11. Hosokawa A, Hirose N, Ueda T, Furumoto T (2014) High-quality machining of CFRP with high helix end mill. CIRP Ann-Manuf Technol 63(1):89–92
12. Hintze W, Hartmann D, Schütte C (2011) Occurrence and propagation of delamination during the machining of carbon fibre reinforced plastics (CFRPs)—an experimental study. Compos Sci Technol 71(15):1719–1726
13. Hintze W, Hartmann D (2013) Modeling of delamination during milling of unidirectional CFRP. Procedia CIRP 8:444–449
14. Hintze W, Cordes M, Koerkel G (2015) Influence of weave structure on delamination when milling CFRP. J Mater Process Technol 216:199–205
15. Hocheng H, Tsao CC (2003) Comprehensive analysis of delamination in drilling of composite materials with various drill bits. J Mater Process Technol 140(140):335–339
16. Wang DH, Ramulu M, Arola D (1995) Orthogonal cutting mechanisms of graphite/epoxy composite. Part I: unidirectional laminate. Int J Mach Tools Manuf 35(12):1623–1638
17. Wang XM, Zhang LC (2003) An experimental investigation into the orthogonal cutting of unidirectional fibre reinforced plastics. Int J Machine Tools Manuf 43(10):1015–1022
18. Bhatnagar N, Ramakrishnan N, Naik NK, Komanduri R (1995) On the machining of fiber reinforced plastic (FRP) composite laminates. Int J Mach Tools Manuf 35(5):701–716
19. Zhang LC, Zhang HJ, Wang XM (2001) A force prediction model for cutting unidirectional fiber–reinforced plastics. Mach Sci Technol 5(3):293–305
20. Jahromi AS, Bahr B (2010) An analytical method for predicting cutting forces in orthogonal machining of unidirectional composites. Compos Sci Technol 70(16):2290–2297
21. Budak E (2006) Analytical models for high performance milling. Part I: cutting forces, structural deformations and tolerance integrity. Int J Mach Tools Manuf 46(12–13):1478–1488
22. Schulze V, Becke C, Pabst R (2012) Specific machining forces and resultant force vectors for machining of reinforced plastics. CIRP Ann-Manuf Technol 60(1):69–72
23. Chang CS (2006) Turning of glass-fiber reinforced plastics materials with chamfered main cutting edge carbide tools. J Mater Process Technol 180(1):117–129
24. Chandrasekharan V, Kapoor SG, Devor RE (1995) A mechanistic approach for prediction the cutting forces in drilling: with application to fiber-reinforced composite materials. J Manuf Sci Eng 117(4):559–570
25. Langlela A, Nele L, Maio A (2005) A torque and thrust prediction model for drilling of composite materials. Compos A: Appl Sci Manuf 36(36):83–93
26. Wang H, Sun J, Li J, Lu L, Li N (2016) Evaluation of cutting force and cutting temperature in milling carbon fiber-reinforced polymer composites. Int J Adv Manuf Technol 82(9):1517–1525
27. Slamani M, Chatelain J.F, Hamedanianpour H (2014) Comparison of two models for predicting tool wear and cutting force components during high speed trimming of CFRP. Int J Mater Form 8(2): 305–316
28. Gara S, Fredj R, Naîmi S, Tsoumarev O (2016) Prediction of cutting forces in slotting of multidirectional CFRP laminate. Int J Adv Manuf Technol DOI. doi:10.1007/s00170-016-9161-8
29. Puw HY, Hocheng H (1999) Milling of polymer composites In: Jahanmir S, Ramulu M (ed) Machining of ceramics and composites. Marcel Dekker Book, p 267–294
30. Wang H, Qin X (2016) A mechanistic model for cutting force in helical milling of carbon fiber-reinforced polymers. Int J Adv Manuf Technol 82(9):1485–1494
31. Sheikh-Ahmad J, Twomey J, Kalla D, Lodhia P (2007) Multiple regression and committee neural network force prediction models in milling FRP. Mach Sci Technol 11(3):391–412
32. Kalla D, Sheikh-Ahmad J, Twomey J (2010) Prediction of cutting forces in helical end milling fiber reinforced polymers. Int J Mach Tools Manuf 50(10):882–891
33. Karpat Y, Bahtiyar O, Değer B (2012) Mechanistic force modeling for milling of unidirectional carbon fiber reinforced polymer laminates. Int J Mach Tools Manuf 56(2):79–93